

THE EVOLUTION OF THE REST-FRAME V-BAND LUMINOSITY FUNCTION FROM $Z = 4$: A CONSTANT FAINT-END SLOPE OVER THE LAST 12 GYR OF COSMIC HISTORY

DANILO MARCHESINI¹, MAURO STEFANON², GABRIEL B. BRAMMER³, AND KATHERINE E. WHITAKER⁴

Accepted to the Astrophysical Journal

ABSTRACT

We present the rest-frame V-band luminosity function (LF) of galaxies at $0.4 \leq z < 4.0$, measured from a near-infrared selected sample constructed from the NMBS, the FIRES, the FIREWORKS, and the ultra-deep NICMOS and WFC3 observations in the HDFN, HUDF, and GOODS-CDFS, all having high-quality optical to mid-infrared data. This unique sample combines data from surveys with a large range of depths and areas in a self-consistent way, allowing us to (1) minimize the uncertainties due to cosmic variance; and (2) simultaneously constrain the bright and faint ends with unprecedented accuracy over the targeted redshift range, probing the LF down to $0.1 L^*$ at $z \sim 3.9$. We find that (1) the faint end is fairly flat and with a constant slope from $z = 4$, with $\alpha = -1.27 \pm 0.05$; (2) the characteristic magnitude has dimmed by 1.3 mag from $z \sim 3.7$ to $z = 0.1$; (3) the characteristic density has increased by a factor of ~ 8 from $z \sim 3.7$ to $z = 0.1$, with 50% of this increase from $z \sim 4$ to $z \sim 1.8$; and (4) the luminosity density peaks at $z \approx 1 - 1.5$, increasing by a factor of ~ 4 from $z = 4.0$ to $z \approx 1 - 1.5$, and subsequently decreasing by a factor of ~ 1.5 by $z = 0.1$. We find no evidence for a steepening of the faint-end slope with redshift out to $z = 4$, in contrast with previous observational claims and theoretical predictions. The constant faint-end slope suggests that the efficiency of stellar feedback may evolve with redshift. Alternative interpretations are discussed, such as different masses of the halos hosting faint galaxies at low and high redshifts and/or environmental effects.

Subject headings: galaxies: evolution — galaxies: formation — galaxies: fundamental parameters — galaxies: high-redshift — galaxies: luminosity function, mass function

1. INTRODUCTION

In the current paradigm of structure formation, dark matter (DM) halos build up in a hierarchical fashion through the dissipationless mechanism of gravitational instability. The assembly of the stellar content of galaxies is instead governed by much more complicated physical processes, often dissipative and non-linear, which are generally poorly understood. To counter this lack of understanding, simplified analytical prescriptions of complex physical processes are employed in galaxy formation models. One of the fundamental tools to constrain the free parameters of these models is the luminosity function (LF), as its shape retains the imprint of galaxy formation and evolution processes.

The underlying physical processes that shape the faint end of the LF are generally associated with feedback from supernovae that is effective in heating gas and driving winds in shallow gravitational potentials (Dekel & Silk 1986). Suppression of gas cooling in low-mass halos due to a background of photo-ionizing radiation also contributes in shaping the faint end (e.g., Benson et al. 2002). Matching the bright end of the LF has proven more challenging. Recent implementation of active galactic nucleus (AGN) feedback in semi-analytic models has yielded faithful reproductions of the observed local rest-frame optical and near-infrared global LFs (e.g., Granato et al. 2004; Bower et al. 2006; Croton et al. 2006; Menci et al. 2006; Kang et al. 2006; Monaco et al. 2007; Somerville et al. 2008). These models provide good matches to the LFs out to $z \sim 1.5$ (e.g., Somerville et al. 2011; and

references therein), although significant disagreements with observations are still present at $z \gtrsim 2$ (e.g., Henriques et al. 2011).

Within the hierarchical structure formation paradigm, one naturally expects strong evolution with redshift of the faint-end slope with steeper slopes at earlier time, considering that the slope of the dark matter mass function is very steep ($\alpha_{\text{DM}} \sim -2$), and that the objects that form in these halos continue to grow by continued star formation and mergers with each other (e.g., Khochfar & Burkert 2001), hence flattening the slope.

Observationally, evidence of evolution of the faint-end slope α has been recently claimed, with α steepening with redshift (Ryan et al. 2007). Khochfar et al. (2007) have shown that simulations of galaxy formation and evolution are able to reproduce the observed redshift evolution of α . Specifically, while supernova feedback is responsible for flatter α with respect to α_{DM} at any given redshift, its evolution with redshift appears to be driven by a steeper dark matter mass function at early cosmic times for the range of halo masses hosting sub- L^* galaxies (e.g., Khochfar et al. 2007; Kobayashi et al. 2007).

Despite the significant improvements in constraining the faint-end of the rest-frame UV LF of dropout galaxies out to $z \sim 8$ (e.g., Oesch et al. 2010b; Bouwens et al. 2011; and references therein), the faint-end slope of the rest-frame optical LFs of galaxies at $z \gtrsim 1$ from near-infrared (NIR) selected samples, which arguably allow for the assembly of representative samples of high-redshift galaxies, is still quite uncertain. Moreover, the evidence of a steepening of α with redshift comes from several surveys, each with unique selection effects, observational biases, and measured at different rest-frame wavelengths. Specifically, all measurements at $z > 3.5$ come from studies in the rest-frame far-UV, whereas at $z \lesssim 3$ LFs are typically measured in the rest-frame optical.

¹ Department of Physics and Astronomy, Tufts University, Medford, MA 02155, USA

² Observatori Astronòmic Universitat de València, C/ Catedrático Agustín Escardino Benlloch, 7, 46980, Valencia, Spain

³ European Southern Observatory (ESO), Santiago, Chile

⁴ Department of Astronomy, Yale University, New Haven, CT 06520, USA

In this paper, we derive the rest-frame optical (V -band) LFs of galaxies over the redshift interval $0.4 \leq z < 4.0$ using a NIR-selected composite sample of galaxies constructed from the NMBS, the FIRES, the GOODS-CDFS surveys, and ultra-deep *Hubble Space Telescope* (HST) data that self-consistently combines the advantages of deep, pencil beam surveys with those of shallow, wider surveys. This NIR composite sample allows us to (1) minimize the uncertainties due to cosmic variance, and empirically quantify its contribution to the total error budget by exploiting the large number of independent field of views; and (2) simultaneously constrain the bright and faint ends of the LF with unprecedented accuracy and statistics over the entire targeted redshift range. This paper is structured as follows. In Section 2, we present the composite NIR-selected sample used to measure the LFs of galaxies at $0.4 \leq z < 4.0$; the methods used to measure the LF (the $1/V_{\max}$ and the maximum likelihood methods) are presented in Section 3, as well as the LFs of galaxies at $0.4 \leq z < 0.7$, $0.76 \leq z < 1.1$, $1.1 \leq z < 1.5$, $1.5 \leq z < 2.1$, $2.1 \leq z < 2.7$, $2.7 \leq z < 3.3$, and $3.3 \leq z < 4.0$, and the evolution of the Schechter function parameters and luminosity density. Our results are summarized in Section 4. We assume $\Omega_M = 0.3$, $\Omega_\Lambda = 0.7$, and $H_0 = 70 \text{ km s}^{-1} \text{ Mpc}^{-1}$. All magnitudes are in the AB system.

2. THE NIR COMPOSITE SAMPLE

The data set we use to measure the LF consists of a composite NIR-selected sample of galaxies built from several multi-wavelength surveys, all having high-quality UV to mid-infrared photometry: the Faint InfraRed Extragalactic Survey (FIRES; Franx et al. 2003), the Great Observatories Origins Deep Survey (GOODS; Giavalisco et al. 2004), the NEWFIRM Medium-Band Survey (NMBS; van Dokkum et al. 2009), the ultra-deep NICMOS observations over the HDF-North (HDFN) GOODS field (Dickinson et al. 1999; Thompson et al. 1999), the ultra-deep WFC3/IR observations taken as part of the HUDF09 program (GO 11563; PI: Illingworth) over the Hubble Ultra-Deep Field (HUDF), and the wide-area WFC3 Early Release Science (ERS) observations over the CDF-South GOODS field (GO 11359; PI: O’Connell).

For the FIRES, GOODS-CDFS, and NMBS surveys we have adopted the publicly-available K -band selected catalogs from Labbé et al. (2003), Wuyts et al. (2008), and Whitaker et al. (2011), respectively. We refer to these works for a complete description of the observations, reduction procedures, and the construction of the K -selected multiwavelength catalogs. Briefly, the FIRES-HDFS catalog (HDFS, hereafter) has 833 sources down to $K_S^{\text{tot}} = 26.0$ over an area of $2.5' \times 2.5'$. The FIREWORKS-CDFS (CDFS, hereafter) K_S -selected catalog comprises 6308 objects down to $K_S^{\text{tot}} = 24.6$ over a total surveyed area of 138 arcmin^2 . The NMBS (COSMOS and AEGIS, hereafter) K -selected catalogs comprise 31,306 and 27,572 objects, respectively, down to $K_S^{\text{tot}} = 24.5$ and over a total surveyed area of 0.5 deg^2 .

For the remaining fields, we have constructed H_{160} -selected catalogs following previous studies (e.g., Labbé et al. 2003). The full details of the reduction, source detection, and generation of the photometric catalogs will be described in Stefanon et al. (2012, in prep.). Briefly, similarly to the other adopted catalogs, we have used SExtractor (Bertin & Arnouts 1996) in dual-image mode, with fluxes measured in the registered and PSF-matched images in order to derive accurate colors and limit any bandpass-dependent effects. We have used an

alternative source fitting algorithm especially suited for heavily confused images for which a higher resolution prior (in this case, the H_{160} -band image) is available to extract the photometry from the IRAC images. This method is described in more detail in the appendix of Marchesini et al. (2009). The UDF WFC3 (UDF, hereafter), GOODS-CDFS WFC3 (ERS, hereafter), and the HDFN NICMOS (HDFN, hereafter) H_{160} -selected catalogs comprise 2100, 9470, and 1774 objects down to $H_{160} = 28.5$, $H_{160} = 27.3$, and $H_{160} = 28.0$, over an area of 5.3, 46.2, and 6.7 arcmin^2 , respectively.

Table 1 provides a summary of the catalogs used, including the filters that each field has been imaged with, the observed K - and H -band limiting magnitudes adopted to construct the composite sample ($K_{\text{lim}}^{\text{tot}}$ and $H_{\text{lim}}^{\text{tot}}$; see § 2.1), the effective area of each pointing (A_{eff}), the number of galaxies over the redshift interval $0.4 < z < 4.0$ used to measure the rest-frame V -band LFs ($N_{0.4 < z < 4.0}$), and the corresponding fraction of galaxies with spectroscopic redshift (f_{zspec}). For the HST H_{160} -selected catalogs, A_{eff} represents the area in the fields where the NIR observations are at least 10% of their maximum depths in the field, and with full coverage in the ACS bands. For the HDFS and FIREWORKS catalogs, A_{eff} represents the area in the fields over which the optical and NIR observations are at least 20% of their maximum depths in the field, following suggested criteria by Labbé et al. (2003) and Wuyts et al. (2008).⁵ Finally, for the NMBS catalogs, A_{eff} represents the area in the fields over which the optical and NIR observations are at least 30% of their maximum depths in the field, again following suggested criteria by Whitaker et al. (2011). The regions around bright stars were also excluded in the calculation of the LF, as faint galaxies in these regions are either obscured by the foreground star or have systematically incorrect magnitudes due to scattered light.

2.1. Completeness

The H_{160} - and K -band limiting magnitudes listed in Table 1 were chosen following a conservative approach that ensures completeness better than 90% in all catalogs down to the adopted limiting magnitudes. The completenesses for the FIRES and FIREWORKS surveys have been characterized in Labbé et al. (2003) and Wuyts et al. (2008). For these catalogs, we have used the same K -band limiting magnitudes previously adopted in Marchesini et al. (2009).

The completenesses of the NMBS catalogs have been derived in Whitaker et al. (2011). When masking sources, the point-source completeness is better than 90% at $K_S^{\text{tot}} < 23.2$. When objects are not masked, objects can fall on or close to other sources, and these blended objects are not properly handled by SExtractor. In this case, the completeness in COSMOS and AEGIS is better than 85 and 87% at $K_S^{\text{tot}} < 22.7$ and 22.8, respectively. However, in our work we have adopted the “de-blended” catalogs, for which these completeness limits are quite conservative (Whitaker et al. 2011). To derive robust limiting magnitudes for the NMBS de-blended catalogs used in our work, we have used the raw number counts of galaxies, which do not show any signs of incompleteness down to $K_S^{\text{tot}} \approx 22.8$, implying completeness better than 95% in the de-blended NMBS catalogs at $K_S^{\text{tot}} < 22.7$ and 22.8 for COSMOS and AEGIS, respectively. Therefore, we have adopted $K_S^{\text{tot}} = 22.7$ and $K_S^{\text{tot}} = 22.8$ for COSMOS and AEGIS, respectively, as the limiting magnitudes to construct the NIR-

⁵ The area of FIREWORKS listed in Table 1 excludes the area covered by the ERS and the UDF catalogs.

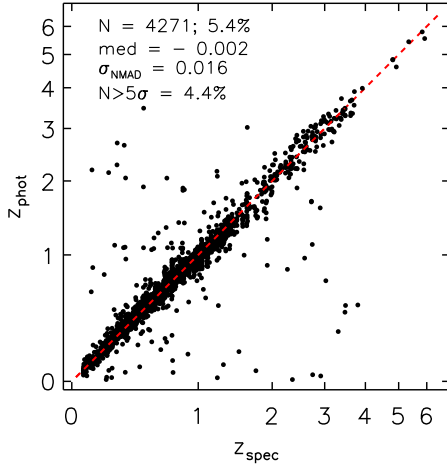


FIG. 1.— Spectroscopic vs. photometric redshifts for the NIR-selected catalogs, shown on a “pseudo-log” scale. The number and fraction of sources with spectroscopic redshifts used in the shown comparison are also specified, as well as the median in $\Delta z/(1+z_{\text{spec}})$, σ_{NMAD} , and the fraction of catastrophic outliers. The comparison between z_{spec} and z_{phot} is extremely good, both at low and high redshifts.

selected composite sample.

The completenesses for the HST H_{160} -selected catalogs (UDF, HDFN, and ERS) will be presented in detail in Stefanon et al. (2012; in prep.). Briefly, the completeness in each catalog was derived following the method in Whitaker et al. (2011). The (point-source) completeness was estimated as a function of magnitude by attempting to recover simulated sources within the H_{160} -band noise-equalized detection image. The derived completeness is better than 90% at $H_{160} < 28.2$, 26.7, and 26.6 for the UDF, ERS, and HDFN catalogs, respectively. We have therefore adopted the conservative limiting magnitudes listed in Table 1, to construct the NIR-selected composite sample.

2.2. Photometric Redshifts

The overall fraction of sources with spectroscopic redshifts in the H_{160} - and K -selected catalogs is 5.4%. Consequently, we must rely primarily on photometric redshift estimates. Photometric redshifts z_{phot} for all galaxies were derived using the EAZY photometric redshift code (Brammer et al. 2008), adopting z_{peak} as the photometric redshift, which finds discrete peaks in the redshift probability function and returns the peak with the largest integrated probability. The template set used in this work is described in Whitaker et al. (2011), composed of EAZY default templates and an additional template for an old, red galaxy. We quantify the accuracy of the photometric redshifts z_{phot} by comparing them to the available spectroscopic redshifts z_{spec} , as shown in Figure 1.

The spectroscopic redshifts for the NMBS COSMOS and AEGIS catalogs were taken from the zCOSMOS survey (Lilly et al. 2007) and the Deep Extragalactic Evolutionary Probe 2 (Davis et al. 2003), respectively. Spectroscopic redshifts of 117 Lyman break galaxies at $z \sim 3$ within the AEGIS field were also added from Steidel et al. (2003). For FIRES and FIREWORKS we used the spectroscopic redshifts compiled in Rudnick et al. (2003) and Wuyts et al. (2008), respectively. For the UDF and ERS H_{160} -selected catalogs, spectroscopic redshifts were taken from the “CDFs Master Catalog” of spectroscopic redshifts (v2.0; I. Balestra; Decem-

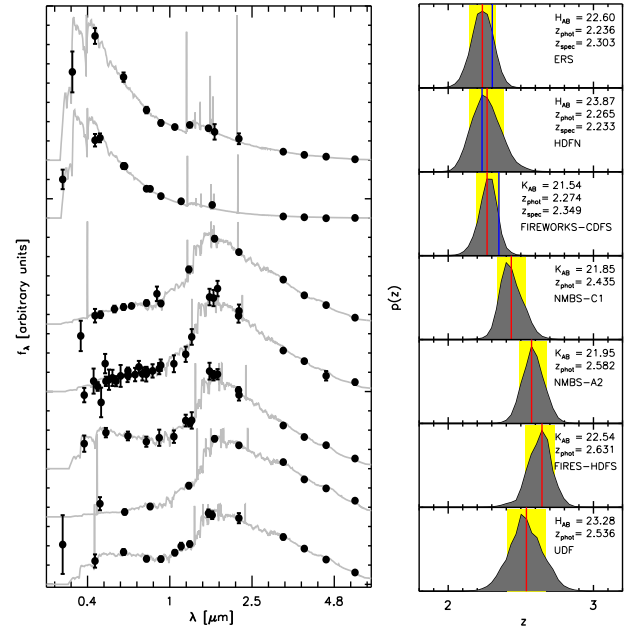


FIG. 2.— *Left*: SEDs of galaxies at $2.1 < z < 2.7$ taken from the seven NIR-selected catalogs used to construct the composite sample: ERS, HDFN, FIREWORKS CDFS, NMBS COSMOS, NMBS AEGIS, FIRES HDFS, and UDF (from top to bottom). The galaxies were arbitrarily selected to have photometric redshifts falling in the targeted redshift interval, with reasonably well-behaved redshift probability functions. They are not representative of the galaxy population at $2.1 < z < 2.7$. Circles are the observed fluxes in units of F_λ , with 1σ errors. The solid gray curves represent the best-fit EAZY templates; each SED was normalized and offset with respect to the others. *Right*: EAZY redshift probability functions (gray regions). The red line is the adopted redshift from EAZY (z_{peak}); the blue line is the spectroscopic redshift, when available. The yellow regions are the 1σ allowed values for z_{peak} . Also listed are the K - or H -band total magnitudes, z_{peak} , and z_{spec} .

ber 2009).⁶ The spectroscopic redshifts for the HDFN H_{160} -selected catalog were taken from Barger et al. (2008).

The comparison between spectroscopic and photometric redshifts results in excellent z_{phot} estimates. The median in $\Delta z/(1+z_{\text{spec}})$, with $\Delta z = z_{\text{phot}} - z_{\text{spec}}$, is -0.000, -0.002, -0.007, 0.018, -0.005, -0.009, and -0.015 in COSMOS, AEGIS, CDFS, HDFS, HDFN, ERS, and UDF, respectively, with the normalized median absolute deviation σ_{NMAD} ⁷ = 0.008, 0.015, 0.029, 0.040, 0.029, 0.037, 0.039. The fraction of catastrophic outliers (defined as galaxies with $|\Delta z|/(1+z_{\text{spec}}) > 5\sigma_{\text{NMAD}}$) is 4.8%, 3.2%, 2.9%, 1.9%, 2.4%, 3.6%, and 4.6% in COSMOS, AEGIS, CDFS, HDFS, HDFN, ERS, and UDF, respectively. Figure 2 provides examples of spectral energy distributions (SEDs) of galaxies at $2.2 < z < 2.7$ in the seven NIR-selected catalogs, along with their corresponding EAZY redshift probability functions.

The accuracy and reliability of the photometric redshifts estimated for the NMBS survey have been discussed in detail in Whitaker et al. (2011), where excellent agreement with the available spectroscopic redshifts is found. The accuracy of the photometric redshifts estimated in the FIRES and FIREWORKS catalogs have been discussed in detail in Brammer et al. (2008), Wuyts et al. (2008), and Marchesini et al. (2009). A detailed discussion of the qual-

⁶ <http://www.eso.org/sci/activities/projects/goods/MasterSpec>

⁷ The normalized median absolute deviation σ_{NMAD} , defined as $1.48 \times \text{median}[|(\Delta z - \text{median}(\Delta z))/(1+z_{\text{spec}})|]$, is equal to the standard deviation for a Gaussian distribution, and it is less sensitive to outliers than the usual definition of the standard deviation (e.g. Brammer et al. 2008)

TABLE 1. SUMMARY OF CATALOGS USED TO CONSTRUCT THE NIR-SELECTED COMPOSITE SAMPLE

Field/Survey	Selection Band	Filter Coverage	$K/H_{\text{lim}}^{\text{tot}}$ (mag)	A_{eff} (arcmin ²)	$N_{0.4 < z < 4.0}$	f_{zspec} [%]	Ref.
UDF	WFC3 H_{160}	ACS B ₄₃₅ V ₆₀₆ I ₇₇₅ Z ₈₅₀ NICMOS J ₁₁₀ H ₁₆₀ WFC3 Y ₁₀₅ J ₁₂₅ H ₁₆₀ ISAAC K _s , IRAC	27.8	5.1	547	7.9	(1,2,3,4)
ERS	WFC3 H_{160}	ACS B ₄₃₅ V ₆₀₆ I ₇₇₅ Z ₈₅₀ WFC3 UV _{225,275,336} Y ₁₀₅ J ₁₂₅ H ₁₆₀ ISAAC HK _s , IRAC	26.3	42.5	2437	10.1	(3,4,5,6,7)
HDFN	NICMOS H_{160}	ACS B ₄₃₅ V ₆₀₆ I ₇₇₅ Z ₈₅₀ WFPC2 U ₃₀₀ B ₄₅₀ V ₆₀₆ I ₈₁₄ NICMOS J ₁₁₀ H ₁₆₀ , IRAC	26.1	6.7	435	15.6	(4,5,6,8,9,10)
HDFS/FIRES	ISAAC K _s	WFPC2 U ₃₀₀ B ₄₅₀ V ₆₀₆ I ₈₁₄ ISAAC J _s HK _s , IRAC	25.6	4.5	204	8.3	(11,12,13)
CDFS/FIREWORKS	ISAAC K _s	ACS B ₄₃₅ V ₆₀₆ I ₇₇₅ Z ₈₅₀ WFI U ₃₈ BVRI, IRAC	23.2	77.2	689	44.6	(5,14)
AEGIS/NMBS	NEWFIRM K	GALEX FUV ₁₅₀₀ NUV ₂₃₀₀ CFHTLS ugriz NEWFIRM J ₁ J ₂ J ₃ H ₁ H ₂ K WIRCam JHK _s , IRAC	22.8	743	7402	15.9	(15,16)
COSMOS/NMBS	NEWFIRM K	GALEX FUV ₁₅₀₀ NUV ₂₃₀₀ Subaru B _j V _j I _r 'i'z', CFHTLS ugriz Subaru 12 medium-bands NEWFIRM J ₁ J ₂ J ₃ H ₁ H ₂ K WIRCam JHK _s , IRAC	22.7	741	7689	7.3	(15,16)

NOTE. — $K/H_{\text{lim}}^{\text{tot}}$ is the observed K - and H_{160} -band limiting magnitudes adopted to construct the NIR-selected composite sample; A_{eff} is the effective area; $N_{0.4 < z < 4.0}$ is the number of galaxies over the redshift interval $0.4 \leq z < 4.0$ used to measure the rest-frame V -band LFs, and f_{zspec} is the corresponding fraction of galaxies with z_{spec} . The references of the used catalogs and data sets are (1) Thompson et al. (2005), (2) Beckwith et al. (2006), (3) Retzlaff et al. (2010), (4) Stefanon et al. (2012; in prep.), (5) Giavalisco et al. (2004), (6) Dickinson et al. (2003), (7) Damen et al. (2011), (8) Williams et al. (1996), (9) Dickinson et al. (1999), (10) Thompson et al. (1999), (11) Franx et al. (2003), (12) Labbé et al. (2003), (13) Wuyts et al. (2007), (14) Wuyts et al. (2008), (15) van Dokkum et al. (2009), (16) Whitaker et al. (2011).

ity of the photometric redshifts in the H_{160} -selected catalogs in UDF, ERS, and HDFN will be presented in Stefanon et al. (2012; in prep.).

It should be stressed that the assessment of the errors of the photometric redshifts from the z_{phot} versus z_{spec} comparison works only if the spectroscopic sample is a random subset of the photometric sample. This is not true in general, as the currently available spectroscopic samples are heavily weighted toward bright and/or blue, low-redshift galaxies. However, Brammer et al. (2008) showed explicitly that the errors in z_{phot} versus z_{spec} plots are generally consistent with the errors estimated from both Monte Carlo simulations and from the formal errors in the fit, i.e., the confidence intervals output by EAzy correctly describe the deviations from the spectroscopic redshifts. We are therefore confident that the photometric redshift uncertainties returned by EAzy are reliable.

2.3. Rest-frame Luminosities

Rest-frame luminosities are derived by integrating the redshifted rest-frame filter bandpass from the best-fit EAzy template, as described in Brammer et al. (2011). This method produces very similar rest-frame luminosities as other methods interpolating between the observed bands that bracket the rest-frame band at a given redshift (e.g., Rudnick et al. 2003). Specifically, down to the H_{160} - and K -band limiting magnitudes of the NIR-selected composite sample, the difference between the rest-frame V -band magnitudes derived with the two methods are very small, ~ 0.02 mag, and no dependence on the H_{160} - or K -band magnitude. We note that most galaxies in the NIR-selected composite sample have robust photome-

try in the IRAC bands⁸, which allows us to properly model the rest-frame optical SEDs of galaxies and to robustly derive their rest-frame V -band magnitudes out to the highest targeted redshift. We computed rest-frame luminosities in the V pass-band defined by Maíz Apellániz (2006). In all cases where a spectroscopic redshift is available, we computed the rest-frame luminosity fixed at z_{spec} .

2.4. The Composite Sample

We constructed a composite NIR-selected sample of galaxies over the redshift range $0.4 \leq z < 4.0$ to be used in the derivation of the rest-frame V -band LFs of galaxies in § 3. The final composite sample includes 19403 NIR-selected galaxies with $H_{160}^{\text{tot}} < 27.8$ or $K^{\text{tot}} < 25.6$, and $0.4 \leq z < 4.0$ over an effective area of 1620 arcmin². Of these sources, 12.5% have spectroscopic redshifts. This NIR-selected sample is unique in that it combines data from surveys with a large range of depths and areas in a self-consistent way. The wide, fairly deep, NMBS survey, with its exquisite photometric redshifts, provides optimal sampling of the bright end of the LF down to the characteristic magnitude at $z \sim 3$ and a factor of ~ 20 fainter than the characteristic luminosity, L^* , at $z \sim 0.6$. The ultra-deep H_{160} -selected catalogs allowed us to probe the faint end down to $0.1 L^*$ at $z \sim 3.9$, and to $0.003 L^*$ at $z \sim 1$ (see also Figure 3).

3. THE LUMINOSITY FUNCTION AND DENSITY

⁸ For the NIR-selected composite sample, 4.1% of the sources at $0.4 \leq z < 4.0$ have IRAC signal-to-noise ratio (S/N) < 3 in the $3.6 \mu\text{m}$ band. This fraction is only slightly larger (5.5%) in the highest targeted redshift interval $3.3 \leq z < 4.0$.

3.1. Methodology and Uncertainties

To estimate the rest-frame V -band LF in the case of a composite sample, we have used the extended version of the $1/V_{\max}$ estimator as defined in Avni & Bahcall (1980). The Poisson error in each magnitude bin was computed adopting the recipe of Gehrels (1986). The $1/V_{\max}$ estimator has the advantages of simplicity and no a priori assumption of a functional form for the LF; it also yields a fully normalized solution. However, it can be affected by the presence of clustering in the sample. Uncertainties due to field-to-field variations in the determination of the LF with the $1/V_{\max}$ method were estimated following the procedure presented in Marchesini et al. (2007), and added in quadrature to the Poisson errors. The contribution from cosmic variance to the error budget is typically 0.06 dex at the characteristic magnitude in all targeted redshift intervals, except at $3.3 \leq z < 4.0$, where it increases to 0.1 dex.

We also measured the LF using the STY method (Sandage, Tammann & Yahil 1979), which is a parametric maximum likelihood estimator. The STY method is unbiased with respect to density inhomogeneities (e.g., Efstathiou, Ellis & Peterson 1988), it has well-defined asymptotic error properties (e.g., Kendall & Stuart 1961), and it does not require binning of the data. For the STY method, we have assumed that the LF is described by a Schechter (1976) function,

$$\Phi(M) = (0.4 \ln 10) \Phi^* \left[10^{0.4(M^* - M)(1+\alpha)} \right] \cdot \exp \left[-10^{0.4(M^* - M)} \right], \quad (1)$$

where α is the faint-end slope parameter, M^* is the characteristic absolute magnitude, and Φ^* is the normalization. The best-fit solution is obtained by maximizing the likelihood Λ with respect to the parameters α and M^* . The value of Φ^* is then obtained by imposing a normalization on the best-fit LF such that the total number of observed galaxies in the sample is reproduced. We have added in quadrature the contribution from cosmic variance previously derived (i.e., 0.06 dex at $z < 3.3$ and 0.1 dex at $3.3 \leq z < 4.0$) to the error budget of Φ^* .

The uncertainties on the LF due to photometric redshift errors have been estimated following the recipe in Marchesini et al. (2009, 2010). Briefly, for each galaxy in the NIR-selected sample, a set of 200 mock SEDs was created by perturbing each flux point according to its formal error bar. Second, photometric redshifts and rest-frame V -band luminosities were estimated as described in § 2. Finally, the LFs were derived with the $1/V_{\max}$ and the STY method for each of the 200 Monte Carlo realizations of the NIR-selected sample. This approach naturally addresses the fact that fainter sources tend to be characterized by less accurate z_{phot} estimates due to the larger errors in their photometry, as well as sources characterized by power-law SEDs and consequently by very poorly constrained z_{phot} estimates and very broad z_{phot} distributions derived from the Monte Carlo realizations.⁹

⁹ We note that catastrophic outliers in the photometric redshift distribution could potentially cause systematic errors in the LF measurements (e.g., Chen et al. 2003). Marchesini et al. (2007) performed extensive simulations to assess the impact of catastrophic outliers on the derived Schechter function parameters, showing that catastrophic outliers will result in measured LFs that are typically steeper than the true LFs, and with brighter characteristic luminosities. For example, at $z > 2$, they found $\Delta\alpha = -0.01$ and $\Delta M^* = -0.05$ mag when the effect of 5% catastrophic outliers is simulated,

The rest-frame V -band LFs of galaxies were derived in the following redshift intervals: $0.4 \leq z < 0.7$, $0.76 \leq z < 1.1$, $1.1 \leq z < 1.5$, $1.5 \leq z < 2.1$, $2.1 \leq z < 2.7$, $2.7 \leq z < 3.3$, and $3.3 \leq z < 4.0$. For all but the lowest redshift interval, the full NIR-selected composite sample was used. In the redshift interval $0.4 \leq z < 0.7$, only the NMBS K -selected samples were used, as the volumes probed by the other surveys become too small to be meaningful. We have excluded the redshift interval $0.7 \leq z < 0.76$, as known clusters of galaxies are present in the COSMOS and CDFS fields (e.g., Guzzo et al. 2007; Trevese et al. 2007; Salimbeni et al. 2009), contaminating the field galaxy LFs presented in this paper.

Because of the coupling between the two parameters α and M^* , the luminosity density (obtained by integrating the LF over all magnitudes) is a robust way to characterize the evolution of the LF with redshift. The luminosity density ρ_L was calculated using

$$\rho_L = \int_0^\infty L_\nu \Phi(L_\nu) dL_\nu = \Gamma(2+\alpha) \Phi^* L^*, \quad (2)$$

which assumes that the Schechter parameterization of the observed LF is a good approximation and valid also at luminosities fainter than probed by our composite sample. The uncertainties on the luminosity density were calculated using the approach adopted in Marchesini et al. (2009). Specifically, the 1σ errors on the total luminosity density have been estimated by deriving the distribution of all of the values of ρ_L allowed within the 1σ solutions of the Schechter function parameters from the maximum likelihood analysis. The contributions to the total error budget from photometric redshift random uncertainties (derived with the Monte Carlo simulations) and from cosmic variance (i.e., 0.06 dex at $z < 3.3$ and 0.1 dex at $3.3 \leq z < 4.0$) were also added in quadrature.

3.2. Results

The rest-frame V -band LFs of galaxies at $0.4 \leq z < 0.7$, $0.76 \leq z < 1.1$, $1.1 \leq z < 1.5$, $1.5 \leq z < 2.1$, $2.1 \leq z < 2.7$, $2.7 \leq z < 3.3$, and $3.3 \leq z < 4.0$ are shown in Figure 3. Also plotted are the LFs in the rest-frame $0.1r$ band (similar to our rest-frame V band) at $z \sim 0.1$ from the Sloan Digital Sky Survey Sixth Data Release (SDSS DR6; Montero-Dorta & Prada 2009) and the Galaxy and Mass Assembly (GAMA) survey (Loveday et al. 2011), to show the evolution from $z = 0.55$ down to $z \sim 0.1$. Note that the local LFs from Montero-Dorta & Prada (2009) and Loveday et al. (2011) are essentially identical. Figure 4 shows the evolution with redshift of the best-fit values and the 1σ and 2σ confidence contour levels of the two Schechter function parameters α and M_V^* derived with the maximum likelihood analysis.

The large surveyed area provided by the NMBS catalogs allows for the determination of the bright end of the rest-frame optical LFs of galaxies at $z > 1$ with unprecedented accuracy, while the depth of the H_{160} -selected catalogs in UDF, HDFN, and ERS allowed us to constrain the faint-end slope out to $z \sim 3.5$, representing a significant improvement with respect to previous works. Specifically, the NMBS samples the LF down to the characteristic magnitude at $z \sim 3$, and down to \sim

much smaller than the random uncertainties on the Schechter function parameters. Whereas it is likely that these systematics effects get larger at lower redshift, especially for the characteristic luminosity, by scaling the results from the simulations in Marchesini et al. (2007), we expect these systematic effects to be in general smaller than, or at most comparable to, the derived random uncertainties on the Schechter function parameters at $z < 1$.

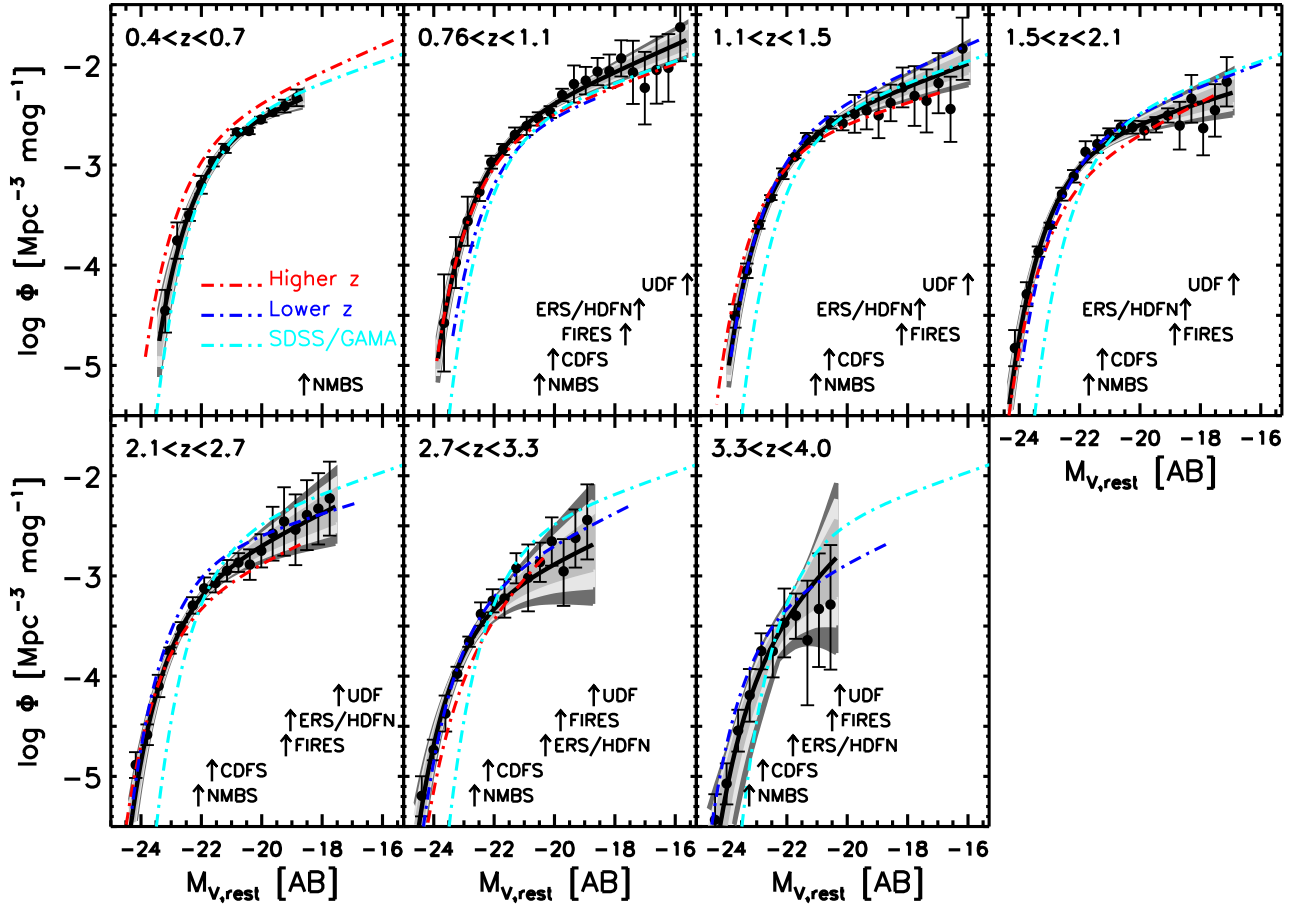


FIG. 3.— Rest-frame V-band LFs of galaxies at $0.4 \leq z < 4.0$. Black filled circles are the $1/V_{\max}$ method estimates with total $1-\sigma$ error bars. The black solid curves are the LFs estimated with the maximum-likelihood method. The shaded gray regions represent the 1-, 2-, and 3- σ uncertainties of the LF estimated from the maximum-likelihood method. The blue and red dot-dashed curves show the LFs measured in the adjacent lower and higher redshift interval, to highlight the evolution with redshift of the LF. The dot-dashed cyan curve represents the local ($z \sim 0.1$) LFs in the rest-frame $0.1r$ band (similar to our rest-frame V band) from the SDSS (Montero-Dorta & Prada 2009) and the GAMA survey (Loveday et al. 2011). The vertical arrows indicate the approximate 90% completeness in rest-frame V-band magnitude of the catalogs used in our work.

$0.05 L^*$ at $z \sim 0.6$, while the ultra-deep H_{160} -selected catalogs allowed us to probe the faint end down to $\sim 0.1 L^*$ at $z \sim 3.9$, and to $\sim 0.003 L^*$ at $z \sim 1$. The approximate completeness in rest-frame V-band magnitude of the catalogs used in our work are indicated in Figure 3 with arrows. Most importantly, the constructed NIR composite sample allowed us to measure, for the first time, the rest-frame optical LF of galaxies from $z = 4.0$ using a single, self-consistent NIR composite sample that fully probes both the bright and the faint ends of the LF over the entire targeted redshift range $0.4 \leq z < 4.0$.

Table 2 lists the derived Schechter function parameters and the estimated luminosity densities in the targeted redshift intervals. Figure 5 shows the evolution with redshift of the Schechter function parameters α , M_V^* , and Φ^* , as well as the evolution with redshift of the luminosity density. Figure 5 also shows the rest-frame V-band Schechter function parameters and luminosity densities derived in other works from the literature, i.e., the Century Survey (Brown et al. 2001), the SDSS (Blanton et al. 2003), the VIMOS-VLT Deep Survey (VVDS; Ilbert et al. 2005), the MUSYC-FIREWORKS-FIRES surveys (Marchesini et al. 2007), the Cosmic Evolution Survey (COSMOS; Liu et al. 2008), the SDSS-DR6 (Montero-Dorta & Prada 2009), and the most recent GAMA survey (Loveday et al. 2011).

The faint-end slope α appears to evolve little with redshift. The weighted average of our measurements and the $z \sim 0.1$ value from the GAMA survey (identical to the SDSS DR6) is $\alpha = -1.27 \pm 0.05$, shown in Figure 5 by the solid blue line and the shaded gray region. Adopting the simple linear fit presented in Ryan et al. (2007) ($\alpha(z) = a + bz$), we find $a = -1.26 \pm 0.02$ and $b = -0.02 \pm 0.03$ (plotted as a black solid line in Figure 5) using the measurements from our work and from Loveday et al. (2011) in the fitting analysis. This is consistent with a constant faint-end slope in the rest-frame V band over the redshift range $0 < z < 4$.¹⁰

We have also modeled the evolution with redshift of the characteristic magnitude M_V^* and the normalization Φ^* using the parameterization presented in Stefanon & Marchesini (2011). Specifically, the following parameterization was adopted to model the observed evolution of M_V^* :

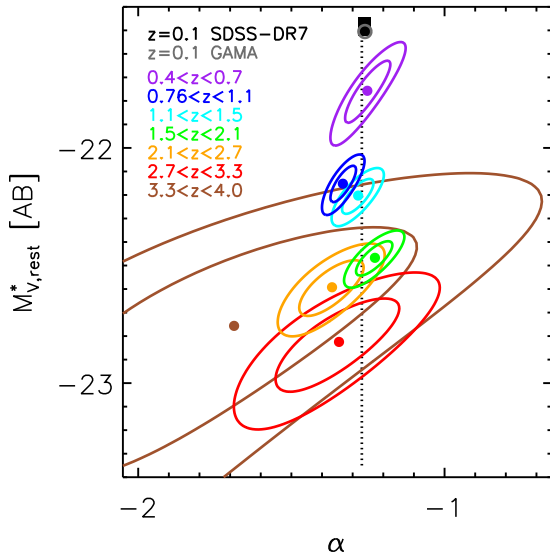
$$M_V^*(z) = \mu [(1+z)/(1+z^*)]^\eta \exp[-(1+z)/(1+z^*)], \quad (3)$$

with μ , z^* , and η free parameters to be determined. By performing a least-square fit to our measurements and from

¹⁰ If only the points from our work are used in the fitting analysis, we obtain $a = -1.30 \pm 0.06$ and $b = 0.00 \pm 0.05$, with a resulting weighted mean $\alpha = -1.29 \pm 0.05$, quantitatively consistent with the analysis including the $z \sim 0.1$ value.

TABLE 2. BEST-FIT SCHECHTER FUNCTION PARAMETERS AND LUMINOSITY DENSITIES

Redshift	M_V^* (mag)	α	Φ^* ($10^{-4} \text{ Mpc}^{-3} \text{ mag}^{-1}$)	$\log \rho_L$ ($\text{erg s}^{-1} \text{ Mpc}^{-3} \text{ Hz}^{-1}$)
$0.4 \leq z < 0.7$	$-21.76^{+0.13}_{-0.14}$	-1.25 ± 0.07	$25.61^{+5.64}_{-3.33}$	$26.85^{+0.09}_{-0.10}$
$0.76 \leq z < 1.1$	$-22.15^{+0.08}_{-0.08}$	-1.33 ± 0.04	$26.16^{+3.33}_{-4.40}$	$27.06^{+0.07}_{-0.07}$
$1.1 \leq z < 1.5$	$-22.20^{+0.07}_{-0.08}$	-1.28 ± 0.05	$22.25^{+3.79}_{-3.83}$	$26.99^{+0.07}_{-0.08}$
$1.5 \leq z < 2.1$	$-22.47^{+0.07}_{-0.08}$	-1.23 ± 0.06	$18.05^{+3.02}_{-3.07}$	$26.97^{+0.07}_{-0.08}$
$2.1 \leq z < 2.7$	$-22.59^{+0.11}_{-0.12}$	-1.37 ± 0.11	$9.82^{+2.87}_{-2.19}$	$26.83^{+0.10}_{-0.11}$
$2.7 \leq z < 3.3$	$-22.83^{+0.18}_{-0.21}$	-1.35 ± 0.20	$6.22^{+2.12}_{-1.97}$	$26.72^{+0.16}_{-0.18}$
$3.3 \leq z < 4.0$	$-22.76^{+0.40}_{-0.63}$	$-1.69^{+0.58}_{-0.66}$	$4.04^{+4.60}_{-3.21}$	$26.8^{+1.5}_{-1.2}$

NOTE. — The quoted errors correspond to the 1σ errors estimated from the maximum likelihood analysis, including the contribution from cosmic variance and from photometric redshift uncertainties.FIG. 4.— (α, M_V^*) parameter space derived from the maximum likelihood analysis. Filled circles are the best-fit values of α and M_V^* derived in our work, while the curves represent their 1σ and 2σ contour levels. The black filled square represents the redshift $z \sim 0.1$ value from the SDSS-DR7 (Montero-Dorta & Prada 2009), whereas the empty gray circle represents the redshift $z \sim 0.1$ value from the GAMA survey (Loveday et al. 2011). The dotted line represents the weighted average of the plotted measurements ($\alpha = 1.27 \pm 0.05$).

Loveday et al. (2011), we obtain the following values: $\mu = -28.8 \pm 0.4 \text{ mag}$, $z^* = 191 \pm 338$, and $\eta = (55.5 \pm 17.2) \times 10^{-3}$. The resulting curve is plotted as a solid dark gray curve in Figure 5. The characteristic magnitude is seen to brighten with redshift, from $M_V^* = -21.5 \text{ mag}$ at $z \sim 0.1$ to $M_V^* = -22.8 \text{ mag}$ at $z \sim 3.7$.

The following parameterization was adopted to model the observed evolution of Φ^* :

$$\Phi^*(z) = \theta \exp[\gamma/(1+z)^\beta], \quad (4)$$

where θ , γ , and β are the free parameters. The best-fit values are $\theta = (3.2 \pm 0.4) \times 10^{-3} \text{ mag}^{-1} \text{ Mpc}^{-3}$, $\gamma = (-4.3 \pm 5.0) \times 10^{-2}$, and $\beta = -2.65 \pm 0.88$. The best-fit of Equation 4 is plotted as a solid dark gray curve in Figure 5. The normalization is seen to increase with cosmic time, by a factor of $\sim 6^{+32}_{-4}$ from $z \sim 3.7$ to $z \sim 0.6$, and by a factor of $\sim 8^{+33}_{-4}$ to $z \sim 0.1$, with 50% of such increase in the 2 Gyr from $z = 4$ to $z = 1.8$,

and the remaining increase in the following 9 Gyr from $z = 1.8$ to $z = 0.1$.

Using the expressions of Eq. 4 and Eq. 3 in Eq. 2, we can derive a functional representation of the luminosity density. The dashed dark gray curve in the bottom panel of Figure 5 represents the luminosity density obtained with this method and adopting the best-fit values of the parameters previously recovered. The agreement with the points is good over the entire redshift range. We stress that no fitting was performed using the luminosity density estimates. The luminosity density appears to peak at $z \approx 1 - 1.5$, increasing by a factor of ~ 4 from $z \sim 3.7$ to $z \sim 1 - 1.5$, and subsequently decreasing by a factor of ~ 1.5 to $z \sim 0.1$.

4. SUMMARY AND CONCLUSIONS

In this paper, we have measured the rest-frame V -band LFs of galaxies at $0.4 \leq z < 4.0$ from a composite NIR-selected sample constructed with the deep NMBS, the FIREWORKS, the very deep FIRES, and the ultra-deep HST optical and NIR data over the HUDF, HDFN, and GOODS-CDFS fields, all having high-quality optical-to-MIR data. This sample is unique as it combines, in a self-consistent way, the advantages of deep, pencil beam surveys with those of shallow, wider surveys, allowing us to (1) minimize the uncertainties due to cosmic variance, and empirically quantify its contribution to the total error budget; and (2) simultaneously constrain the bright and faint ends of the rest-frame optical LFs with unprecedented accuracy over the entire targeted redshift range.

The main results of our derivation of the rest-frame V -band LF of galaxies from $z = 4.0$ are (1) the faint-end slope remains fairly flat and does not seem to evolve from $z = 4$ to $z = 0$, consistent with $\alpha = -1.27 \pm 0.05$; (2) the characteristic magnitude has dimmed by 1 mag from $M_V^* = -22.8$ at $z \sim 3.7$ to $M_V^* = -21.8$ at $z \sim 0.6$, and by $\sim 1.3 \text{ mag}$ to $z = 0.1$; (3) the normalization Φ^* has increased by a factor of ~ 6 from $z \sim 3.7$ to $z \sim 0.6$, and by a factor of ~ 8 to $z = 0.1$; and (4) the luminosity density peaks at $z \approx 1 - 1.5$, increasing by a factor of ~ 4 from $z = 4.0$ to $z \approx 1 - 1.5$, and subsequently decreasing by a factor of ~ 1.5 by $z = 0.1$.

In contrast with the findings of Ryan et al. (2007), we find weak, if any, evidence for a steepening of the faint-end slope with redshift out to $z = 4$. The top panel of Figure 5 shows the best-fit model derived in Ryan et al. (2007) (dot-dashed line). Using the simple linear fit $\alpha(z) = a + bz$, Ryan et al. (2007) found $b \approx -0.12$, whereas we find $b = -0.02 \pm 0.03$, consistent with no evolution with redshift of the rest-frame V -band faint-end slope over the redshift range $0.4 \leq z < 4.0$. We note that

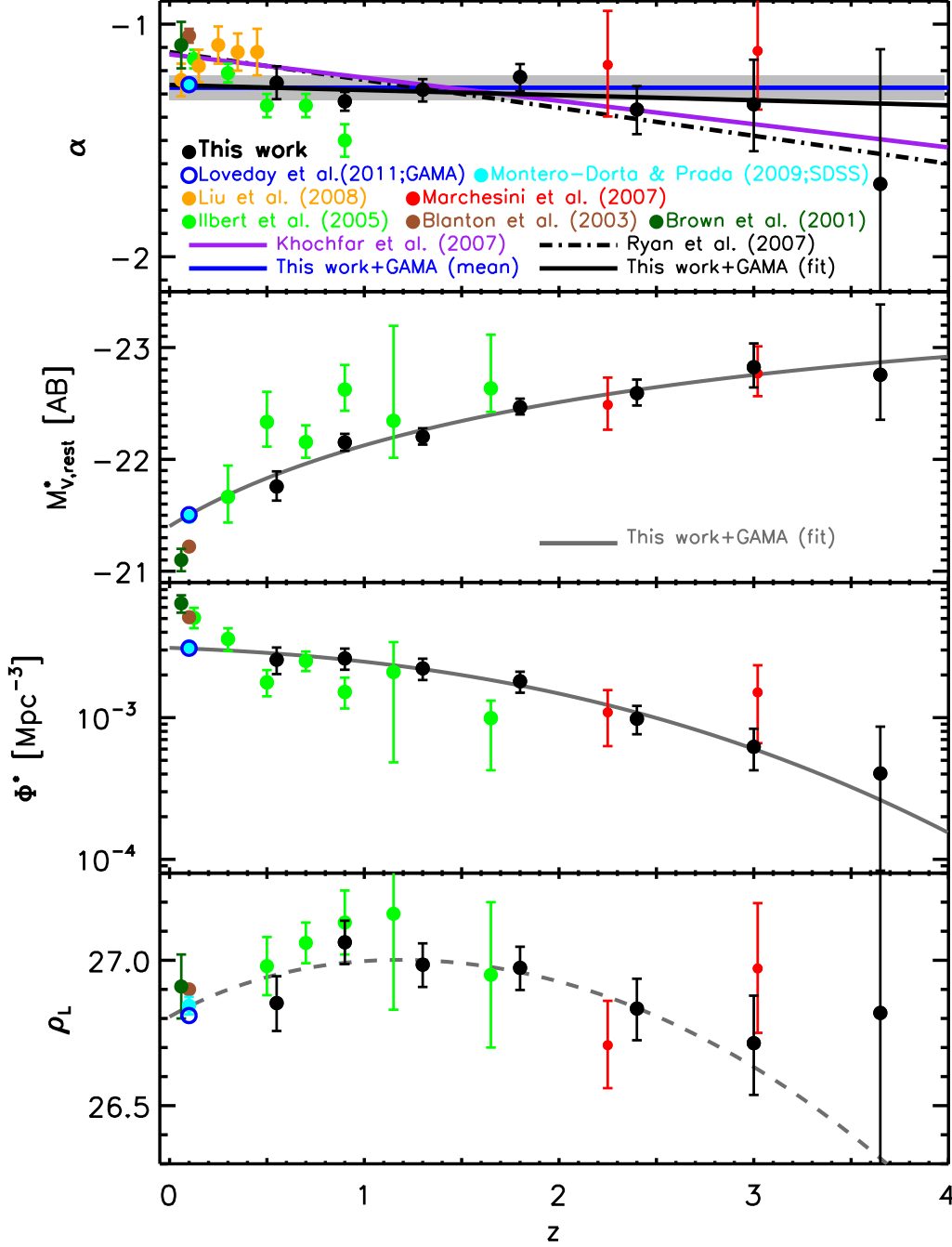


FIG. 5.— Evolution of the Schechter (1976) function parameters (α , M_V^* , and Φ^* , top three panels), and the luminosity density (bottom panel) with redshift. Filled black circles are the values derived in this work. Filled dark green, green, red, and orange circles are the values from Brown et al. (2001), Ilbert et al. (2005), Marchesini et al. (2007), and Liu et al. (2008), respectively. The open blue and filled cyan circles represent the rest-frame $^{0.1}r$ -band (similar to our rest-frame V band) results at $z \sim 0.1$ from the GAMA survey (Loveday et al. 2011) and the SDSS DR6 (Montero-Dorta & Prada 2009), respectively. The filled brown circle represents the SDSS rest-frame $^{0.1}r$ -band results at $z \sim 0.1$ from Blanton et al. (2003). The blue line in the top panel shows the weighted mean of the faint-end slopes from our work and Loveday et al. (2011), with the gray shaded area representing the error of the mean. The purple line is the theoretical prediction from Khochfar et al. (2007), whereas the dot-dashed black line is the best-fit model derived in Ryan et al. (2007); the solid black line represents the best fit derived by fitting the values of α from Loveday et al. (2011) and our work with $\alpha(z) = a + bz$. The solid dark gray curves represent the best-fits of the evolution with redshift of M_V^* and Φ^* (using the parameterizations introduced in Stefanon & Marchesini 2011; see § 3.2) using the values from Loveday et al. (2011) and our work. The dashed dark gray curve in the bottom panel is obtained adopting the best-fit curves of the evolution with redshift of M_V^* and Φ^* into Eq. 2.

the evolution of the faint-end slope with redshift presented in Ryan et al. (2007) was found by combining measurements of the faint-end slopes in the rest-frame B and UV bands. When only the rest-frame B -band values are considered, the evolution of the faint-end slope with redshift becomes marginal.

While the rest-frame B and V bands are close enough that significant differences should not be expected, we cannot exclude systematic differences in the (evolution) of the faint-end slopes in different rest-frame optical bands. It should be finally noted that a steepening in the faint-end slope at $z \gtrsim 2.5$

might still be present, due to the large uncertainties on the faint-end slope at $z > 3$.

The hierarchical formation scenario states that many dwarf galaxies at high redshifts will undergo merging over time. This implies a steeper faint-end slope at higher redshifts. Using semi-analytical modeling of galaxy formation, Khochfar et al. (2007) investigated the evolution with redshift of the rest-frame B -band faint-end slope of the LF, finding $b \approx -0.1$, in good agreement with the results from Ryan et al. (2007). The predicted evolution of α from Khochfar et al. (2007) is also plotted in Figure 5 (purple line). Our measurements are consistent with no evolution of the faint-end slope over the last 12 Gyr of cosmic history, in apparent contrast with what is expected in the current paradigm of structure formation. Supernova feedback is thought to be mainly responsible for a flatter faint-end slope compared to the dark matter halo mass slope α_{DM} at any given redshift (Dekel & Silk 1986), with α_{DM} flattening with cosmic time, as shown by Λ CDM numerical simulations (e.g., Reed et al. 2003). A constant α from $z = 4$ would then imply either no evolution in α_{DM} in the last 12 Gyr, in contrast with Λ CDM simulations, or a redshift-dependent efficiency of stellar feedback, with supernova feedback being more efficient at higher redshifts when α_{DM} is also steeper. Alternatively, the non-evolving rest-frame V -band faint-end slope out to $z = 4$ could be explained while maintaining a constant stellar feedback efficiency, if we assumed that the galaxies at the faint end are hosted by different dark matter halos at different redshifts. In other words, the observed faint galaxies at low redshifts are hosted by more massive dark matter halos compared to similarly faint galaxies at high redshifts. Additionally, systematic effects could be introduced by the sampled environments of faint galaxies, if these environments vary systematically at different redshifts. In fact, as shown by Khochfar et al. (2007), α is steeper and evolves more strongly in field environments than in cluster environments. Consequently, if the faint-end of the LF at high redshifts is observationally dominated by present-day cluster members, the faint-end slope of the overall galaxy population at high redshifts would then be flatter than that for the field LF alone at the same redshift, potentially resulting in the observed little or no evolution with redshift of α .

Whereas we find a fairly flat and constant faint-end slope from $z = 4$ in the rest-frame V band, significantly steeper slopes are consistently found in the rest-frame far-UV, both at $z > 4$ ($\alpha \lesssim -1.7$; e.g., Bouwens et al. 2007; Ouchi et al. 2009;

Oesch et al. 2010a; Bouwens et al. 2011; Lee et al. 2011) and at $z < 4$ ($\alpha \sim -1.6$; Arnouts et al. 2005; Reddy & Steidel 2009; Hathi et al. 2010; Oesch et al. 2010b). Our NIR composite sample will allow us to study the evolution of the LFs from $z = 4$ at different rest-frame wavelengths, from the far-UV to the NIR, and to investigate the wavelength-dependence of the faint-end slope and its potentially different varying evolution with redshift in different rest-frame wavebands.

We stress that we have measured the *observed* rest-frame V -band LFs over the targeted redshift range $0.4 \leq z < 4.0$. No attempt was made to infer the intrinsic, dust-corrected, rest-frame V -band LF of galaxies, which is beyond the scope of our work. We note however that, similar to what has been found in the local universe (e.g., Driver et al. 2007), internal dust extinction is likely to play a significant role in shaping the observed LF, especially in the early universe where larger amount of dust extinction is typically found, even in galaxies around the characteristic mass (e.g., Marchesini et al. 2010; Brammer et al. 2011).

The ongoing *Hubble Space Telescope* CANDELS (Grogin et al. 2011; Koekemoer et al. 2011) and 3D-HST (van Dokkum et al. 2011; Brammer et al. 2012) surveys, once completed, will result in significantly improved constraints at the faint end, providing 1) very deep data over an area larger by a factor > 10 with respect to the area surveyed by the ultra deep HST data used in this work, and 2) spectroscopic redshifts for thousands of faint galaxies, significantly reducing the uncertainties due to photometric redshift errors.

We thank the anonymous referee for helpful comments and suggestions that significantly improved the manuscript. We thank Lars Hernquist for helpful discussions. This study makes use of data from the NEWFIRM Medium-Band Survey, a multi-wavelength survey conducted with the NEWFIRM instrument at the KPNO, supported in part by the NSF and NASA. The authors acknowledge support from programs HST-AR-11764.04 and HST-AR-12141.01, provided by NASA through a grant from the Space Telescope Science Institute, which is operated by the Association of Universities for Research in Astronomy, Incorporated, under NASA contract NAS5-26555. Based on observations made with ESO Telescopes at the La Silla or Paranal Observatories under programme ID(s): 66.A-0270, 67.A-0418, 074.A-0709, 164.O-0560, 170.A-0788, 171.A-3045, and 275.A-5060.

REFERENCES

- Arnouts, S., et al. 2005, *ApJ*, 619, L43
 Avni, Y., & Bahcall, J. N. 1980, *ApJ*, 235, 694
 Barger, A. J., Cowie, L. L., & Wang, W.-H. 2008, *ApJ*, 689, 687
 Beckwith, S. V. W., et al. 2006, *AJ*, 132, 1729
 Benson, A. J., Lacey, C. G., Baugh, C. M., Cole, S., & Frank, C. S. 2002, *MNRAS*, 333, 156
 Bertin, E., & Arnouts, S. 1996, *A&A*, 117, 393
 Blanton, M. R., et al. 2003, *ApJ*, 592, 819
 Brammer, G. B., van Dokkum, P. G., & Coppi, P. 2008, *ApJ*,
 Brammer, G. B., et al. 2011, *ApJ*, 739, 24
 Brammer, G. B., et al. 2012, *ApJ* submitted
 Bouwens, R. J., Illingworth, G. D., Franx, M., & Ford, H. 2007, *ApJ*, 670, 928
 Bouwens, R. J., et al. 2011, *ApJ*, 737, 90
 Bower, R. G., Benson, A. J., Malbon, R., Helly, J. C., Frenk, C. S., Baugh, C. M., Cole, S., & Lacey, C. G. 2006, *MNRAS*, 370, 645
 Brown, W. R., Geller, M. J., Fabricant, D. G., & Kurtz, M. J. 2001, *AJ*, 122, 714
 Chen, H.-W., et al. 2003, *ApJ*, 586, 745
 Croton, D. J., et al. 2006, *MNRAS*, 365, 11
 Damen, M., et al. 2011, *ApJ*, 727, 1
 Davis, M., et al. 2003, *Proc. SPIE*, 4834, 161
 Dekel, A., & Silk, J. 1986, *ApJ*, 303, 39
 Dickinson, M. 1999, *AIP Conf. Proc.*, 470, 122
 Dickinson, M., et al. 2003, in *The Mass of Galaxies at Low and High Redshift: Proc. European Southern Observatory and Universitäts-Sternwarte München Workshop, ESO Astrophysics Symp.*, ed. R. Bender & A. Renzini (Berlin: Springer), 324
 Driver, S. P., et al. 2007, *MNRAS*, 379, 1022
 Efstathiou, G., Ellis R. S., & Peterson, B. A. 1988, *MNRAS*, 232, 431
 Franx, M., et al. 2003, *ApJ*, 587, L79
 Gehrels, N. 1986, *ApJ*, 303, 336
 Giavalisco, M., et al. 2004, *ApJ*, 600, L93
 Granato, G. L., De Zotti, G., Silva, L., Bressan, A., & Danese, L. 2004, *ApJ*, 600, 580
 Grogin, N. A., et al. 2011, *ApJS*, 197, 35
 Guzzo, L., et al. 2007, *ApJS*, 172, 254
 Hathi, N. P., et al. 2010, *ApJ*, 720, 1708
 Henriques, B., White, S. D. M., Lemson, G., Thomas, P., Guo, Q., Marleau, G.-D., Overzier, R. 2011, *MNRAS* submitted, [arXiv:1109.3457]

- Ilbert, O., et al. 2005, A&A, 439, 863
- Kang X., Jing Y. P., Silk J., 2006, ApJ, 648, 820
- Kendall, M. G., & Stuart, A. 1961, *The Advanced Theory of Statistics*, Vol. 2, Griffin & Griffin, London
- Khochfar, S., & Burkert, A. 2001, ApJ, 561, 517
- Khochfar, S., Silk, J., Windhorst, R. A., & Ryan, R. E. Jr. 2007, ApJ, 668, L115
- Kobayashi, C., Springel, V., & White, S. D. M. 2007, MNRAS, 376, 1465
- Koekemoer, A. M., et al. 2011, ApJS, 197, 36
- Labbé, I., et al. 2003, AJ, 125, 1107
- Lee, K.-S., et al. 2011, ApJ submitted [arXiv:1111.1233]
- Lilly, S. J., et al. 2007, ApJS, 172, 70
- Liu, C. T., et al. 2008, ApJ, 672, 198
- Loveday, J., et al. 2011, MNRAS in press [arXiv:1111.0166]
- Maíz Apellániz, J. 2006, AJ, 131, 1184
- Marchesini, D. et al. 2007, ApJ, 656, 42
- Marchesini, D. et al. 2009, ApJ, 701, 1765
- Marchesini, D. et al. 2010, ApJ, 725, 1277
- Menci N., Fontana A., Giallongo E., Grazian A., Salimbeni S., 2006, ApJ, 647, 753
- Monaco P., Fontanot F., Taffoni G., 2007, MNRAS, 375, 1189
- Montero-Dorta, A. D., & Prada, F. 2009, MNRAS, 399, 1106
- Oesch, P. A., et al. 2010a, ApJ, 709, L16
- Oesch, P. A., et al. 2010b, ApJ, 725, L150
- Ouchi, M., et al. 2009, ApJ, 706, 1136
- Reddy, N. A., & Steidel, C. C. 2009, ApJ, 692, 778
- Reed, D., et al. 2003, MNRAS, 346, 565
- Retzlaff, J., et al. 2010, A&A, 511, 50
- Rudnick, G., et al. 2003, ApJ, 599, 847
- Ryan, R. E., Jr., et al. 2007, ApJ, 668, 839
- Salimbeni, S., et al. 2009, A&A, 501, 865
- Sandage, A., Tammann, G. A., & Yahil, A. 1979, ApJ, 232, 352
- Schechter, P. 1976, ApJ, 203, 297
- Somerville R. S., Hopkins P. F., Cox T. J., Robertson B. E., Hernquist L., 2008, MNRAS, 391, 481
- Somerville, R. S., Gilmore, R. C., Primack, J. R., Domínguez, A. 2011, MNRAS submitted [arXiv:1104.0669]
- Stefanon, M., & Marchesini, D. 2011, MNRAS submitted [arXiv:1112.0006]
- Steidel, C. C., Adelberger, K. L., Shapley, A. E., Pettini, M., Dickinson, M., & Giavalisco, M. 2003, ApJ, 592, 728
- Thompson, R. I., et al. 1999, AJ, 117, 17
- Thompson, R. I., et al. 2005, AJ, 130, 1
- Trevese, D., Castellano, M., Fontana, A., & Giallongo, E. 2007, A&A, 463, 853
- van Dokkum, P. G. 2009, PASP, 121, 2
- van Dokkum, P. G., et al. 2011, ApJ, 743, L15
- Whitaker, K. E., et al. 2010, ApJ, 719, 1715
- Whitaker, K. E., et al. 2011, ApJ, 735, 86
- Williams, R. E., et al. 1996, AJ, 112, 4
- Wuyts, S., et al. 2007, ApJ, 655, 51
- Wuyts, S., et al. 2008, ApJ, 682, 985